



A new photosensitive neuron model and its dynamics^{*}

Yong LIU¹, Wan-jiang XU¹, Jun MA^{†‡2,3}, Faris ALZHRANI⁴, Aatef HOBINY⁴

¹*School of Mathematics and Statistics, Yancheng Teachers University, Yancheng 224002, China*

²*Department of Physics, Lanzhou University of Technology, Lanzhou 730050, China*

³*School of Science, Chongqing University of Posts and Telecommunications, Chongqing 430065, China*

⁴*NAAM-Research Group, Department of Mathematics, King Abdulaziz University, Jeddah 21589, Saudi Arabia*

[†]E-mail: hyperchaos@163.com; hyperchaos@lut.edu.cn

Received Nov. 9, 2019; Revision accepted Jan. 25, 2020; Crosschecked Mar. 31, 2020; Published online Apr. 21, 2020

Abstract: Biological neurons can receive inputs and capture a variety of external stimuli, which can be encoded and transmitted as different electric signals. Thus, the membrane potential is adjusted to activate the appropriate firing modes. Indeed, reliable neuron models should take intrinsic biophysical effects and functional encoding into consideration. One fascinating and important question is the physical mechanism for the transcription of external signals. External signals can be transmitted as a transmembrane current or a signal voltage for generating action potentials. We present a photosensitive neuron model to estimate the nonlinear encoding and responses of neurons driven by external optical signals. In the model, a photocell (phototube) is used to activate a simple FitzHugh-Nagumo (FHN) neuron, and then external optical signals (illumination) are imposed to excite the photocell for generating a time-varying current/voltage source. The photocell-coupled FHN neuron can therefore capture and encode external optical signals, similar to artificial eyes. We also present detailed bifurcation analysis for estimating the mode transition and firing pattern selection of neuronal electrical activities. The sampled time series can reproduce the main characteristics of biological neurons (quiescent, spiking, bursting, and even chaotic behaviors) by activating the photocell in the neural circuit. These results could be helpful in giving possible guidance for studying neurodynamics and applying neural circuits to detect optical signals.

Key words: Photosensitive neuron; Neuron model; Bifurcation; Bursting; Photocell

<https://doi.org/10.1631/FITEE.1900606>

CLC number: TN710; O59

1 Introduction

The nervous system consists of many functional units that process signals and encode information. To carry out their function, neurons must be sensitive to different stimuli and respond appropriately and rapidly. In generic neuron models (Gu and Pan, 2015; Hu et al., 2016; Mondal and Upadhyay, 2018; Hu and Liu, 2019; Wang YH et al., 2019), external forcing includes physical current forcing, acoustical signals,

audio signals, electromagnetic radiation (Duan et al., 2018; Ye et al., 2018; Meng et al., 2019; Takembo et al., 2019a, 2019b), noise (Hauschildt et al., 2006; Richardson and Swarbrick, 2010; Wu et al., 2017), and optical signals. These external stimuli are often described by their equivalent transmembrane currents or induction currents (Upadhyay et al., 2017; Xu Y et al., 2018b), which can change neuronal membrane potentials and induce a variety of neuronal firing patterns and oscillation modes. Based on some of these neuron models, standard bifurcation analysis can be used to reproduce the main dynamical properties of neuronal electrical activities and to predict when the bursting synchronization (Batista et al., 2013; Jia et al., 2018; Rakshit et al., 2018c) and neuronal disease (Hagell et al., 2002; Seifert and Steinhäuser, 2013) might occur. Furthermore,

[‡] Corresponding author

^{*} Project supported by the National Natural Science Foundation of China (No. 11672122) and the Hongliu First-Class Disciplines Development Program of Lanzhou University of Technology, China

ORCID: Yong LIU, <https://orcid.org/0000-0002-9387-5417>; Jun MA, <https://orcid.org/0000-0002-6127-000X>

© Zhejiang University and Springer-Verlag GmbH Germany, part of Springer Nature 2020

astrocytes have been coupled to connect neurons to build reliable neuron-astrocyte networks to estimate the biological function of astrocytes (Postnov et al., 2009; Nazari et al., 2015; Pankratova et al., 2019).

From the dynamical viewpoint, many nonlinear oscillators can be activated to reproduce firing patterns in biological neurons, specifically by applying external periodical forces and selecting excitation parameters. Han et al. (2014, 2015, 2018) and Yu Y et al. (2017) conducted several instructive studies to investigate mode transitions, fast-slow analysis of time delay effects, and frequency excitation effects on nonlinear oscillators. Therefore, most dynamical systems can be tamed by applying periodical stimulation or adjusting excitation parameters. Using these methods, spiking, bursting, and even chaotic behaviors can be generated to reproduce the main dynamical properties of electrical activities in biological neurons. Furthermore, many neural circuits (Erokhin et al., 2011; Haghiri et al., 2016; Pham et al., 2016; Nair et al., 2017; Xu F et al., 2018) can be developed using these theoretical neuron-like oscillators by a variety of nonlinear electric components. Indeed, this physical effect becomes important when building neuron models, because an electromagnetic field is induced in the cell when the density of intracellular and extracellular ions changes, such as when supplying the channel current for generating action potential firing patterns. Therefore, magnetic flux and memristive synapses (Park et al., 2015; Wu et al., 2016; Rajagopal et al., 2019) have been introduced into neuron models, and the effect of electromagnetic induction (Ge et al., 2018; Wu et al., 2019) has been estimated by calculating the induction current across cell membrane. To further understand this physical effect, electric field variables (Ma J et al., 2019a) have been used to build new biophysical neuron models. Modeling field coupling (Xu Y et al., 2018a, 2019; Lv et al., 2019) between neurons helps describe signal exchange and propagation across neural networks. In fact, when neurons are connected with a capacitive synapse, e.g., when neural circuits are coupled by a capacitor which propagates signals between neurons (Liu et al., 2019), electric field coupling is activated. When neurons are connected with an inductive synapse, e.g., when neural circuits are coupled by an inductor (Yu DS et al., 2017; Yao et al., 2019), magnetic field coupling is switched to benefit signal

propagation between neurons. For further details, readers can refer to Ma J et al. (2019b).

As mentioned above, neurons receive synaptic signals in the form of synaptic currents from adjacent neurons. Furthermore, different external stimuli can be converted into synaptic currents via appropriate receptors. For example, photoelectric sensors encode light stimuli with certain frequencies into electric signals, which can activate the visual system. In this study, we present a phototube in the simple FitzHugh-Nagumo (FHN) neuron model (Binczak et al., 2006; Cubero et al., 2006; Gaiko, 2011), which is described as the Bonhoeffer-van der Pol oscillator (Keener, 1983; Kyprianidis et al., 2012). The photocell is used as a reliable voltage/current source and thus supplies the neuron with continuous stimuli.

2 Model, scheme, and discussion

A Bonhoeffer-van der Pol oscillator can be activated to generate bursting and spiking patterns by applying carefully modulated external periodical excitation. Therefore, it is often used to investigate the dynamics of neural activities. When building neural circuits, external forcing can be treated as a voltage source or a current source (Kyprianidis et al., 2012). This simple circuit can be further used to model the synchronization stability between neurons. Because of the physical properties of the phototube, which can convert light into an electrical current, a phototube can be used as a realistic voltage source that excites and regulates neural activities. Inspired by the contributions of Kyprianidis et al. (2012), we select a physical phototube as a voltage source to excite the FHN neural circuit. The circuit is illustrated in Fig. 1.

Characteristics of the nonlinear resistor (NR) connected in the circuit (FitzHugh, 1961; Keener, 1983) are estimated by

$$i_{\text{NR}} = -\frac{1}{\rho} \left(V - \frac{1}{3} \frac{V^3}{V_0^2} \right), \quad (1)$$

where ρ and V_0 are the normalization parameters of the nonlinear resistor and V the output voltage of the capacitor. The photoelectric effect (Brust, 1965; Agostini and Petite, 1988; Georges, 1995) is a

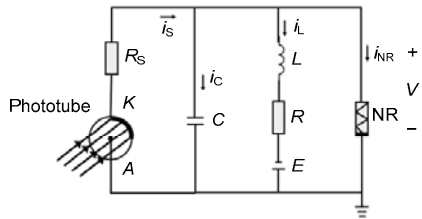


Fig. 1 Implementation of the circuit built for the FitzHugh-Nagumo neuron

A phototube is used to capture external illumination and high-frequency lights, and it activates photocurrents from the phototube and is considered as the voltage source V_s . NR is the nonlinear resistor, C the capacitor, L the induction coil, E the constant voltage source, K the cathode, and A the anode in the phototube

phenomenon in which electrons in some materials are excited by photons to form a current when an electromagnetic wave above a certain frequency is applied. For further experimental physical investigation, a phototube is designed as a voltage source and a control component in nonlinear circuits. A photocell is a basic photoelectric conversion device based on the external photoelectric effect. A photocell can convert light signals into electrical signals in some frequency bands. Photocells are characterized as either vacuum photocells or gas photocells. The typical structure of a photocell is to vacuum the spherical glass shell, to coat the inner hemisphere surface with a layer of photoelectric material as the cathode, and to place a small spherical or annular piece of metal as the anode. If the ball is filled with a low-pressure inert gas, it becomes an inflatable photocell. Photoelectrons collide with gas molecules during their flight to the anode and ionize the gas, which increases the sensitivity of photocells. The metals used as photocathodes include alkali metal, mercury, gold, and silver. Based on experimental tests, the voltage-photocurrent relationship of phototube is shown in Fig. 2.

Using a mathematical approach, the curve in Fig. 2 is estimated using a variety of nonlinear functions as follows:

$$\begin{cases} I_a = \frac{2I_H}{\pi} \arctan(U - U_a), \\ I_b = I_H \frac{\exp(U - U_a) - \exp(U_a - U)}{\exp(U - U_a) + \exp(U_a - U)}, \\ I_c = \frac{I_H}{1 + (I_H - 1)\exp(U_a - U)}. \end{cases} \quad (2)$$

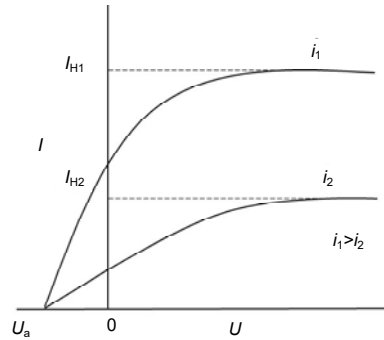


Fig. 2 A plot of the relationship between voltage and photocurrent

U and I represent the voltage and current of the phototube, respectively. I_{H1} and I_{H2} are the maximum currents (saturation currents) emitted from the phototube when the light intensities (i_1 and i_2) are strong enough. U_a denotes the reverse cut-off voltage and is dependent on the material properties of the phototube cathode

That is, three kinds of nonlinear functions can be selected to represent the relationship between the voltage and photocurrent across the phototube. For simplicity and consistency with the variables in Fig. 1, the photocurrent across the phototube is selected as the first type in Eq. (2), and is defined by

$$i_s = \frac{2I_H}{\pi} \arctan(V_s - V_a), \quad (3)$$

where I_H is the maximum current, V_s the output voltage of the phototube, and V_a the normalized parameter associated with the phototube. Guided by the physical Kirchhoff law, the circuit equations in Fig. 1 are obtained by

$$\begin{cases} C \frac{dV}{dt} = \frac{V_s - V}{R_s} - i_L - i_{NR}, \\ L \frac{di_L}{dt} = V + E - Ri_L. \end{cases} \quad (4)$$

The phototube can generate a time-varying forcing current i_s , which is calculated using the transcendental equation as follows:

$$i_s = \frac{2I_H}{\pi} \arctan(V_s - V_a) = \frac{V_s - V}{R_s}. \quad (5)$$

For further dynamical analysis, the physical variables are mapped into dimensionless variables by applying

the scale transformation for the variables and parameters as follows:

$$\begin{cases} x = \frac{V}{V_0}, y = \frac{\rho i_L}{V_0}, \tau = \frac{t}{\rho C}, a = \frac{E}{V_0}, b = \frac{R}{\rho}, \\ c = \frac{\rho^2 C}{L}, \xi = \frac{\rho}{R_s}, u_s = \frac{\rho V_s}{R_s V_0}. \end{cases} \quad (6)$$

As a result, the equivalent FHN neuron driven by the photocurrent can be rewritten by

$$\begin{cases} \frac{dx}{d\tau} = x(1-\xi) - \frac{1}{3}x^3 - y + u_s, \\ \frac{dy}{d\tau} = c(x+a-by). \end{cases} \quad (7)$$

In addition, the variables and parameters are consistent with the definition in Keener (1983), and the parameters are selected as $a=0.8$, $b=0.8$, and $c=0.1$, with the parameter ξ fixed at different values for calculating the firing patterns and nonlinear responses in the FHN neuron driven by the phototube. From the dynamical viewpoint, a broad range of parameters (a , b , c , and ξ) can be selected to generate a variety of firing patterns and oscillations. In a practical way, more phototubes can be connected in parallel, thus enhancing the photocurrent intensity.

In the general case, the driving voltage source has the following form:

$$u_s = A \cos(\omega\tau), \quad (8)$$

where A and ω denote the amplitude and frequency of the excitation, respectively. That is, the phototube can be used as a voltage source for generating a time-varying stimulus, thus activating the neural circuit. According to the known experiments examining the photoelectric effect in phototubes, a photocurrent can be induced in the phototube when the frequency of external illumination is beyond the intrinsic frequency threshold, which is dependent on the material of the phototube cathode. From a dynamical viewpoint, the angular frequency of the photocurrent and the voltage of the phototube can be selected from a large range of values. Indeed, the excitability of this neuron can be adjusted by the external stimulus, which, in turn, regulates its firing patterns and oscillatory modes.

It is important to apply the standard nonlinear stability analysis to this neuron model with the external voltage source removed from system (7), expressed as follows:

$$\begin{cases} \frac{dx}{d\tau} = x(1-\xi) - \frac{1}{3}x^3 - y, \\ \frac{dy}{d\tau} = c(x+a-by), \end{cases} \quad (9)$$

where the dissipativity of this autonomous neuron oscillator is approached by $\nabla V = 1 - \xi - x^2 - bc$. The oscillator becomes dissipative when $1 - \xi - x^2 - bc < 0$. Only one equilibrium point $S_0 = (0, 0)$ is detected by setting $a=0$ and $b(1-\xi)=1$. In the generic case, there are three equilibrium points $S_i = [m_i, (m_i+a)/b]$ ($i=1, 2, 3$). To present the simple form, intermediate parameters are defined as $p=3(b-b\xi-1)/b$, $q=-3a/b$, $\omega=0.5 \cdot (-1+i\sqrt{3})$, and then the form is approached as follows:

$$\begin{cases} m_1 = \left[-\frac{q}{2} + \sqrt{\left(\frac{q}{2}\right)^2 + \left(\frac{p}{3}\right)^3} \right]^{1/3} + \left[-\frac{q}{2} - \sqrt{\left(\frac{q}{2}\right)^2 + \left(\frac{p}{3}\right)^3} \right]^{1/3}, \\ m_2 = \omega \left[-\frac{q}{2} + \sqrt{\left(\frac{q}{2}\right)^2 + \left(\frac{p}{3}\right)^3} \right]^{1/3} + \omega^2 \left[-\frac{q}{2} - \sqrt{\left(\frac{q}{2}\right)^2 + \left(\frac{p}{3}\right)^3} \right]^{1/3}, \\ m_3 = \omega^2 \left[-\frac{q}{2} + \sqrt{\left(\frac{q}{2}\right)^2 + \left(\frac{p}{3}\right)^3} \right]^{1/3} + \omega \left[-\frac{q}{2} - \sqrt{\left(\frac{q}{2}\right)^2 + \left(\frac{p}{3}\right)^3} \right]^{1/3}. \end{cases} \quad (10)$$

Furthermore, there are three real roots under the condition of $9a^2b+4(b-b\xi-1)^3 \leq 0$, while for $9a^2b+4(b-b\xi-1)^3 > 0$, one real root and two complex roots are observed. The properties of these equilibria can be determined using the associated characteristic polynomial as follows:

$$f(\lambda) = \lambda^2 + (bc - 1 + \xi + x^2)\lambda + (1 - b + b\xi + bx^2)c. \quad (11)$$

It can be confirmed that S_0 can be obtained when $b(1-\xi)=1$ and $a=0$, and that S_0 is unstable. Two possible bifurcation sets can be obtained for S_i ($i=1, 2, 3$). One is expressed as

$$S: 1 - b + b\xi + bm_i^2 = 0, \quad i=1, 2, 3, \quad (12)$$

where simple bifurcation (*S*) may occur. The other type can be written as

$$H : c = b^2(1 + c^2), \quad (13)$$

where Hopf bifurcation (*H*) may occur. As a result, when an external voltage source is applied and activated, the equilibrium point will be disturbed, thus inducing instability.

We focus on the influence of the driving photocurrent on the dynamics of the FHN neuron. With the parameters fixed at $a=0.7$, $b=0.8$, $c=0.1$, $\omega=1.004$, and $\zeta=0.175$, the bifurcation diagram with excitation amplitude variation is plotted in Fig. 3, where y represents the value of variable y on the Poincaré projection at $x=-0.5$. Using the Matlab platform, ODE45 is applied to find solutions for the neuron model.

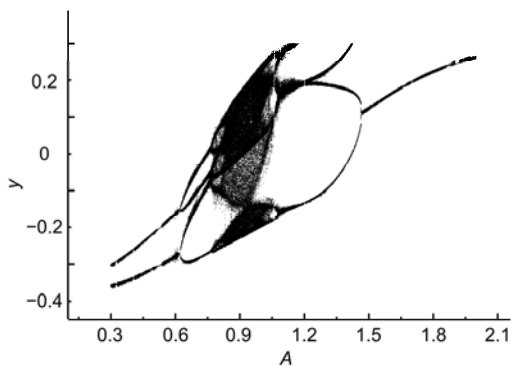


Fig. 3 Bifurcation diagram for $a=0.7$, $b=0.8$, $c=0.1$, $\omega=1.004$, and $\zeta=0.175$
 A is the amplitude of the external stimulus

Appropriate settings for the external stimulus amplitude can induce chaos and bursting firing. In fact, the dynamics are dependent on the selection of intrinsic parameters. Therefore, these parameters are tamed to reveal the mode transition and dynamics selection with parametric excitation (Fig. 4).

We confirm that the cascades of period-doubling bifurcations to chaos are obtained in all the variation processes of the parameters, and that period windows can be detected in the chaotic regions. To better illustrate this, the output series for variables are shown in Figs. 5, 6, and 7 to discern mode oscillations in the quiescent, bursting, and spiking states, respectively.

Fig. 5 shows that the neuron exists in a quiescent state after a certain transient period when the amplitude of the external stimulus is below the excitation

intensity threshold. Then, the external stimulus is changed to trigger a new electrical firing mode, and the results are shown in Fig. 6.

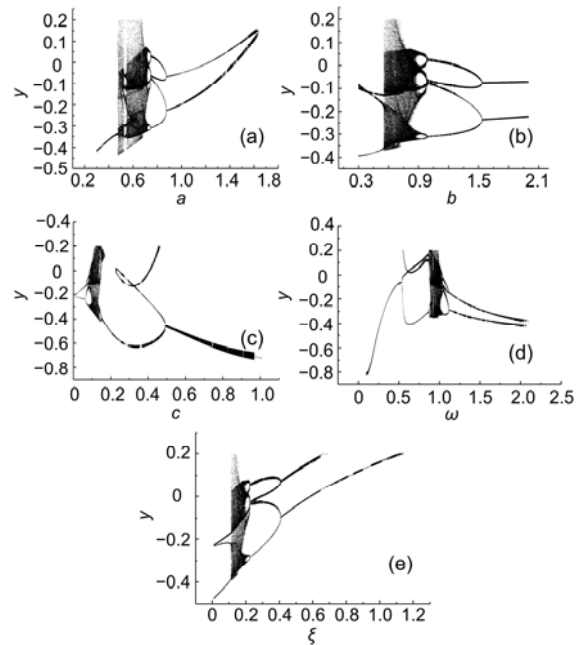


Fig. 4 Bifurcation diagrams calculated by changing the intrinsic parameters ($a, b, c, A, \omega, \zeta$): (a) $b=0.8$, $c=0.1$, $A=0.9$, $\omega=1.004$, $\zeta=0.175$; (b) $a=0.7$, $c=0.1$, $A=0.9$, $\omega=1.004$, $\zeta=0.175$; (c) $a=0.7$, $b=0.8$, $A=0.9$, $\omega=1.004$, $\zeta=0.175$; (d) $a=0.7$, $b=0.8$, $c=0.1$, $A=0.9$, $\zeta=0.175$; (e) $a=0.7$, $b=0.8$, $c=0.1$, $A=0.9$, $\omega=1.004$

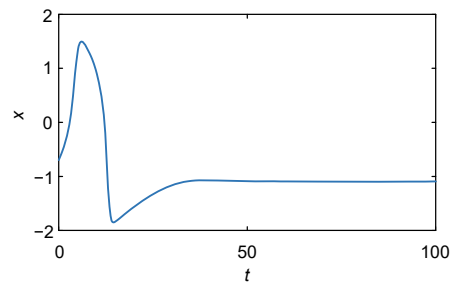


Fig. 5 Transient pulse and quiescent state approached by setting $a=0.7$, $b=0.8$, $c=0.1$, $A=0.03$, $\omega=0.035$, and $\zeta=0.175$

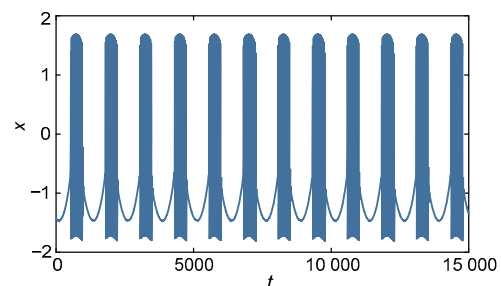


Fig. 6 A continuous bursting pattern generated by setting $a=0.7$, $b=0.8$, $c=0.1$, $A=0.8$, $\omega=0.005$, and $\zeta=0.175$

When the current across the phototube is further increased, the neuron thus presents a continuous bursting pattern, and neural activities show intermittent dense spiking. As spiking patterns are often detected in biological neurons and neural circuits, we further tame the voltage source to excite the neuron, and the firing patterns of spiking are presented in Fig. 7.

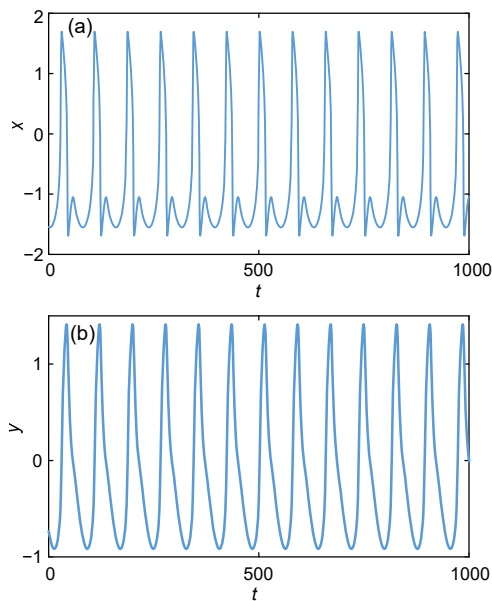


Fig. 7 Continuous spiking patterns generated by setting $a=0.7$, $b=0.8$, $c=0.1$, $A=0.8$, $\omega=0.08$, and $\zeta=0.175$: (a) time series for variable x ; (b) time series for variable y

According to Figs. 5–7, most firing patterns and characteristics of the neural activities can be reproduced in the new neuron model by altering the current of the phototube. Therefore, this neuron is suitable for describing the dynamical response and information encoding of optical signals. The neuron model is oscillator-like, and it shows common periodical and chaotic behaviors generated by many nonlinear oscillators when external forcing is applied. An intuitive illustration is presented in Fig. 8, showing the calculated sampled time series and chaotic attractors.

Appropriate parameter selection can thus trigger chaotic attractors and time series for variables in the neural circuit. According to the bifurcation diagrams, appropriate parameters can be selected to generate chaos. Indeed, the neuronal firing pattern and mode selection are controlled by the intrinsic parameters and external stimulus properties. In particular, the current from the phototube as a reliable voltage

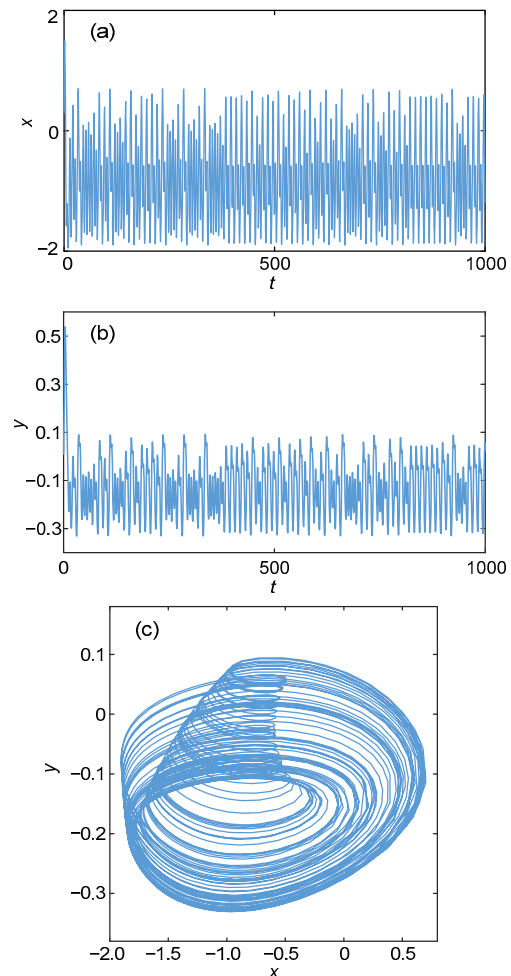


Fig. 8 Sampled time series for variables x (a) and y (b) and formation of the chaotic attractor (c) approached at $a=0.7$, $b=0.8$, $c=0.1$, $A=0.9$, $\omega=1.004$, and $\zeta=0.175$

source can regulate the firing of the neuron. Our results describe the physical mechanism for the information encoding of optical signals. This new neuron can be used to extensively to study the collective behaviors of neural networks. Additionally, analog circuits can be built to reproduce relevant numerical results and synchronization between neurons without direct channel coupling. In a generic way, the standard interspike interval (ISI) is often calculated to estimate possible mode transitions in neural activities using the sampled time-series data from the isolated neuron in neural networks. In particular, ISI-based bifurcation analysis (Rakshit et al., 2018a; Bera et al., 2019) is helpful in prediction and detection of regularity in firing patterns and chimera states in networks with time-varying stimuli and connections. ISI-based bifurcation analysis presents a simple but effective

way to calculate the bifurcation by estimating the dependence of firing patterns and the amplitude of the observable variable on the intrinsic parameter. In this way, standard stability analysis is confirmed using the statistical ISI series.

A variety of electronic components can be used to build neural circuits to model different biophysical functions. To consider the effects of heterogeneous diffusion and electromagnetic induction, a fractional order neuron model (Rajagopal et al., 2019) has been used to discuss the dynamics of neural activities in the presence of electromagnetic radiation. In most studies, researchers match the dynamics analysis with biological experimental data while conducting reliable investigations on how to build functional neural circuits. For example, Ma YQ et al. (2018) presented an interesting and important guidance for decision making using a spiking neural network. When a memristor is included while building neural circuits (Xu Q et al. 2018; Bao B et al., 2019; Bao H et al., 2019; Zhang et al., 2019a, 2019b), the memory field effect can be estimated. The addition of a thermistor in the nonlinear circuit can allow the detection and prediction of slight changes in biological environments. Furthermore, piezoelectric devices can be integrated into nonlinear circuits that allow the detection of slight deformations in the skin and the body. For extensive studies, more functional components can be integrated into functional neural circuits with multi-channel perception. Indeed, when more biological and artificial neurons are included while building neural networks (Bera et al., 2016; Rakshit, 2018b) by applying different topological connections and chimera states (Mostaghimi et al., 2019; Tang et al., 2019), spatial pattern transitions (Uzun et al., 2017; Rostami et al., 2018; Etémé et al., 2019) and synchronization stability (Wang CN et al. 2017) can be studied further. The circuit described in this study is inspired by these interesting works on pattern formation and network synchronization, and can be used to build neural networks for detecting and capturing optical signals.

3 Conclusions

In this study, we proposed a neuron model in which a physical phototube is used as a voltage source. The phototube can capture high-frequency external

optical signals which activate the FHN neuron in a variety of firing patterns that are characteristics of most neural activities, allowing such activities to be reproduced and estimated. Detailed bifurcation and stability analyses were applied to find the mode dependence of the bifurcation parameters and the current from the phototube. When the phototube was activated and tamed, the neural circuit can model a variety of firing patterns. The sampled time series for the membrane potential confirmed this dynamical property. This neuron can be used to further capture and encode optical signals. Furthermore, the neural circuit can be used to build networks for detecting optical signals and estimating collective behaviors of neural networks exposed to illumination. It also provides information for designing artificial eyes for potential therapeutic applications.

Contributors

Jun MA designed the research and drafted the manuscript. Yong LIU and Wan-jiang XU processed the data. Faris AL-ZAHRANI and Aatef HOBINY helped organize the manuscript. Jun MA and Yong LIU revised and finalized the paper.

Compliance with ethics guidelines

Yong LIU, Wan-jiang XU, Jun MA, Faris ALZHRANI, and Aatef HOBINY declare that they have no conflict of interest.

References

- Agostini P, Petite G, 1988. Photoelectric effect under strong irradiation. *Contemp Phys*, 29(1):57-77.
<https://doi.org/10.1080/00107518808213751>
- Bao B, Yang Q, Zhu L, et al., 2019. Chaotic bursting dynamics and coexisting multistable firing patterns in 3D autonomous Morris-Lecar model and microcontroller-based validations. *Int J Bifurc Chaos*, 29(10):1950134.
<https://doi.org/10.1142/S0218127419501347>
- Bao H, Wang N, Wu HG, et al., 2019. Bi-stability in an improved memristor-based third-order Wien-bridge oscillator. *IETE Techn Rev*, 36(2):109-116.
<https://doi.org/10.1080/02564602.2017.1422395>
- Batista CAS, Viana RL, Ferrari FAS, et al., 2013. Control of bursting synchronization in networks of Hodgkin-Huxley-type neurons with chemical synapses. *Phys Rev E*, 87(4):042713.
<https://doi.org/10.1103/PhysRevE.87.042713>
- Bera BK, Ghosh D, Lakshmanan M, 2016. Chimera states in bursting neurons. *Phys Rev E*, 93(1):012205.
<https://doi.org/10.1103/PhysRevE.93.012205>
- Bera BK, Rakshit S, Ghosh D, et al., 2019. Spike chimera states and firing regularities in neuronal hypernetworks. *Chaos*, 29(5):053115.

- <https://doi.org/10.1063/1.5088833>
- Binczak S, Jacquir S, Bilbault JM, et al., 2006. Experimental study of electrical FitzHugh-Nagumo neurons with modified excitability. *Neur Networks*, 19(5):684-693. <https://doi.org/10.1016/j.neunet.2005.07.011>
- Brust D, 1965. Band-theoretic model for the photoelectric effect in silicon. *Phys Rev*, 139(2A):A489. <https://doi.org/10.1103/PhysRev.139.A489>
- Cubero D, Baltanás JP, Casado-Pascual J, 2006. High-frequency effects in the FitzHugh-Nagumo neuron model. *Phys Rev E*, 73(6):061102. <https://doi.org/10.1103/PhysRevE.73.061102>
- Duan LX, Cao QY, Wang ZJ, et al., 2018. Dynamics of neurons in the pre-Bötzinger complex under magnetic flow effect. *Nonl Dynam*, 94(3):1961-1971. <https://doi.org/10.1007/s11071-018-4468-7>
- Erokhin V, Berzina T, Camorani P, et al., 2011. Material memristive device circuits with synaptic plasticity: learning and memory. *BioNanoScience*, 1(1-2):24-30. <https://doi.org/10.1007/s12668-011-0004-7>
- Etémé AS, Tabi CB, Mohamadou A, et al., 2019. Elimination of spiral waves in a two-dimensional Hindmarsh-Rose neural network under long-range interaction effect and frequency excitation. *Phys A*, 533:122037. <https://doi.org/10.1016/j.physa.2019.122037>
- Fitzhugh R, 1961. Impulses and physiological states in theoretical models of nerve membrane. *Biophys J*, 1(6):445-466. [https://doi.org/10.1016/S0006-3495\(61\)86902-6](https://doi.org/10.1016/S0006-3495(61)86902-6)
- Gaiko VA, 2011. Multiple limit cycle bifurcations of the FitzHugh-Nagumo neuronal model. *Nonl Anal Theory Methods Appl*, 74(18):7532-7542. <https://doi.org/10.1016/j.na.2011.08.017>
- Ge MY, Jia Y, Xu Y, et al., 2018. Mode transition in electrical activities of neuron driven by high and low frequency stimulus in the presence of electromagnetic induction and radiation. *Nonl Dynam*, 91(1):515-523. <https://doi.org/10.1007/s11071-017-3886-2>
- Georges AT, 1995. Theory of the multiphoton photoelectric effect: a stepwise excitation process. *Phys Rev B*, 51(19):13735-13738. <https://doi.org/10.1103/PhysRevB.51.13735>
- Gu HG, Pan BB, 2015. A four-dimensional neuronal model to describe the complex nonlinear dynamics observed in the firing patterns of a sciatic nerve chronic constriction injury model. *Nonl Dynam*, 81(4):2107-2126. <https://doi.org/10.1007/s11071-015-2129-7>
- Hagell P, Piccini P, Björklund A, et al., 2002. Dyskinesias following neural transplantation in Parkinson's disease. *Nat Neurosci*, 5(7):627-628. <https://doi.org/10.1038/nn863>
- Haghiri S, Ahmadi A, Saif M, 2016. VLSI implementable neuron-astrocyte control mechanism. *Neurocomputing*, 214:280-296. <https://doi.org/10.1016/j.neucom.2016.06.015>
- Han XJ, Bi QS, Zhang C, et al., 2014. Study of mixed-mode oscillations in a parametrically excited van der Pol system. *Nonl Dynam*, 77(4):1285-1296. <https://doi.org/10.1007/s11071-014-1377-2>
- Han XJ, Bi QS, Ji P, et al., 2015. Fast-slow analysis for parametrically and externally excited systems with two slow rationally related excitation frequencies. *Phys Rev E*, 92(1):012911. <https://doi.org/10.1103/PhysRevE.92.012911>
- Han XJ, Bi QS, Kurths J, 2018. Route to bursting via pulse-shaped explosion. *Phys Rev E*, 98(1):010201(R). <https://doi.org/10.1103/PhysRevE.98.010201>
- Hauschildt B, Janson NB, Balanov A, et al., 2006. Noise-induced cooperative dynamics and its control in coupled neuron models. *Phys Rev E*, 74(5):051906. <https://doi.org/10.1103/PhysRevE.74.051906>
- Hu XY, Liu CX, 2019. Dynamic property analysis and circuit implementation of simplified memristive Hodgkin-Huxley neuron model. *Nonl Dynam*, 97(2):1721-1733. <https://doi.org/10.1007/s11071-019-05100-8>
- Hu XY, Liu CX, Liu L, et al., 2016. An electronic implementation for Morris-Lecar neuron model. *Nonl Dynam*, 84(4):2317-2332. <https://doi.org/10.1007/s11071-016-2647-y>
- Jia B, Wu YC, He D, et al., 2018. Dynamics of transitions from anti-phase to multiple in-phase synchronizations in inhibitory coupled bursting neurons. *Nonl Dynam*, 93(3):1599-1618. <https://doi.org/10.1007/s11071-018-4279-x>
- Keener JP, 1983. Analog circuitry for the van der Pol and FitzHugh-Nagumo equations. *IEEE Trans Syst Man Cybern*, SMC-13(5):1010-1014. <https://doi.org/10.1109/TSMC.1983.6313098>
- Kyprianidis IM, Papachristou V, Stouboulos IN, et al., 2012. Dynamics of coupled chaotic Bonhoeffer-van der Pol oscillators. *WSEAS Trans Syst*, 11(9):516-526.
- Liu ZL, Ma J, Zhang G, et al., 2019. Synchronization control between two Chua's circuits via capacitive coupling. *Appl Math Comput*, 360:94-106. <https://doi.org/10.1016/j.amc.2019.05.004>
- Lv M, Ma J, Yao YG, et al., 2019. Synchronization and wave propagation in neuronal network under field coupling. *Sci China Technol Sci*, 62(3):448-457. <https://doi.org/10.1007/s11431-018-9268-2>
- Ma J, Zhang G, Hayat T, et al., 2019a. Model electrical activity of neuron under electric field. *Nonl Dynam*, 95(2):1585-1598. <https://doi.org/10.1007/s11071-018-4646-7>
- Ma J, Yang ZQ, Yang LJ, et al., 2019b. A physical view of computational neurodynamics. *J Zhejiang Univ-Sci A (Appl Phys & Eng)*, 20(9):639-659. <https://doi.org/10.1631/jzus.A1900273>
- Ma YQ, Wang ZR, Yu SY, et al., 2018. A novel spiking neural network of receptive field encoding with groups of neurons decision. *Front Inform Technol Electron Eng*, 19(1):139-150. <https://doi.org/10.1631/FITEE.1700714>
- Meng FQ, Zeng XQ, Wang ZL, 2019. Dynamical behavior and synchronization in time-delay fractional-order coupled

- neurons under electromagnetic radiation. *Nonl Dynam*, 95(2):1615-1625.
<https://doi.org/10.1007/s11071-018-4648-5>
- Mondal A, Upadhyay RK, 2018. Diverse neuronal responses of a fractional-order Izhikevich model: journey from chattering to fast spiking. *Nonl Dynam*, 91(2):1275-1288.
<https://doi.org/10.1007/s11071-017-3944-9>
- Mostaghimi S, Nazarimehr F, Jafari S, et al., 2019. Chemical and electrical synapse-modulated dynamical properties of coupled neurons under magnetic flow. *Appl Math Comput*, 348:42-56. <https://doi.org/10.1016/j.amc.2018.11.030>
- Nair MV, Muller LK, Indiveri G, 2017. A differential memristive synapse circuit for on-line learning in neuromorphic computing systems. *Nano Fut*, 1(3):035003.
<https://doi.org/10.1088/2399-1984/aa954a>
- Nazari S, Amiri M, Faez K, et al., 2015. Multiplier-less digital implementation of neuron-astrocyte signalling on FPGA. *Neurocomputing*, 164:281-292.
<https://doi.org/10.1016/j.neucom.2015.02.041>
- Pankratova EV, Kalyakulina AI, Stasenko SV, et al., 2019. Neuronal synchronization enhanced by neuron-astrocyte interaction. *Nonl Dynam*, 97(1):647-662.
<https://doi.org/10.1007/s11071-019-05004-7>
- Park S, Chu M, Kim J, et al., 2015. Electronic system with memristive synapses for pattern recognition. *Sci Rep*, 5(1):10123. <https://doi.org/10.1038/srep10123>
- Pham VT, Jafari S, Vaidyanathan S, et al., 2016. A novel memristive neural network with hidden attractors and its circuitry implementation. *Sci China Technol Sci*, 59(3):358-363. <https://doi.org/10.1007/s11431-015-5981-2>
- Postnov DE, Koreshkov RN, Brazhe NA, et al., 2009. Dynamical patterns of calcium signaling in a functional model of neuron-astrocyte networks. *J Biol Phys*, 35(4):425-445. <https://doi.org/10.1007/s10867-009-9156-x>
- Rajagopal K, Nazarimehr F, Karthikeyan A, et al., 2019. Dynamics of a neuron exposed to integer- and fractional-order discontinuous external magnetic flux. *Front Inform Technol Electron Eng*, 20(4):584-590.
<https://doi.org/10.1631/FITEE.1800389>
- Rakshit S, Bera BK, Ghosh D, et al., 2018a. Emergence of synchronization and regularity in firing patterns in time-varying neural hypernetworks. *Phys Rev E*, 97(5):052304. <https://doi.org/10.1103/PhysRevE.97.052304>
- Rakshit S, Bera BK, Ghosh D, 2018b. Synchronization in a temporal multiplex neuronal hypernetwork. *Phys Rev E*, 98(3):032305.
<https://doi.org/10.1103/PhysRevE.98.032305>
- Rakshit S, Ray A, Bera BK, et al., 2018c. Synchronization and firing patterns of coupled Rulkov neuronal map. *Nonl Dynam*, 94(2):785-805.
<https://doi.org/10.1007/s11071-018-4394-8>
- Richardson MJE, Swarbrick R, 2010. Firing-rate response of a neuron receiving excitatory and inhibitory synaptic shot noise. *Phys Rev Lett*, 105(17):178102.
<https://doi.org/10.1103/PhysRevLett.105.178102>
- Rostami Z, Pham VT, Jafari S, et al., 2018. Taking control of initiated propagating wave in a neuronal network using magnetic radiation. *Appl Math Comput*, 338:141-151.
<https://doi.org/10.1016/j.amc.2018.06.004>
- Seifert G, Steinhäuser C, 2013. Neuron-astrocyte signaling and epilepsy. *Exp Neurol*, 244:4-10.
<https://doi.org/10.1016/j.expneurol.2011.08.024>
- Takembo CN, Mvogo A, Fouda HPE, et al., 2019a. Effect of electromagnetic radiation on the dynamics of spatio-temporal patterns in memristor-based neuronal network. *Nonl Dynam*, 95(2):1067-1078.
<https://doi.org/10.1007/s11071-018-4616-0>
- Takembo CN, Mvogo A, Fouda HPE, et al., 2019b. Wave pattern stability of neurons coupled by memristive electromagnetic induction. *Nonl Dynam*, 96(2):1083-1093.
<https://doi.org/10.1007/s11071-019-04841-w>
- Tang J, Zhang J, Ma J, et al., 2019. Noise and delay sustained chimera state in small world neuronal network. *Sci China Technol Sci*, 62(7):1134-1140.
<https://doi.org/10.1007/s11431-017-9282-x>
- Upadhyay RK, Mondal A, Teka WW, 2017. Mixed mode oscillations and synchronous activity in noise induced modified Morris-Lecar neural system. *Int J Bifurc Chaos*, 27(5):1730019.
<https://doi.org/10.1142/S0218127417300191>
- Uzun R, Yilmaz E, Ozer M, 2017. Effects of autapse and ion channel block on the collective firing activity of Newman-Watts small-world neuronal networks. *Phys A*, 486:386-396.
<https://doi.org/10.1016/j.physa.2017.05.049>
- Wang CN, Lv M, Alsaedi A, et al., 2017. Synchronization stability and pattern selection in a memristive neuronal network. *Chaos*, 27(11):113108.
<https://doi.org/10.1063/1.5004234>
- Wang YH, Xu XY, Zhu YT, et al., 2019. Neural energy mechanism and neurodynamics of memory transformation. *Nonl Dynam*, 97(1):697-714.
<https://doi.org/10.1007/s11071-019-05007-4>
- Wu FQ, Wang CN, Xu Y, et al., 2016. Model of electrical activity in cardiac tissue under electromagnetic induction. *Sci Rep*, 6(1):28.
<https://doi.org/10.1038/s41598-016-0031-2>
- Wu FQ, Wang CN, Jin WY, et al., 2017. Dynamical responses in a new neuron model subjected to electromagnetic induction and phase noise. *Phys A*, 469:81-88.
<https://doi.org/10.1016/j.physa.2016.11.056>
- Wu FQ, Ma J, Zhang G, 2019. A new neuron model under electromagnetic field. *Appl Math Comput*, 347:590-599.
<https://doi.org/10.1016/j.amc.2018.10.087>
- Xu F, Zhang JQ, Fang TT, et al., 2018. Synchronous dynamics in neural system coupled with memristive synapse. *Nonl Dynam*, 92(3):1395-1402.
<https://doi.org/10.1007/s11071-018-4134-0>
- Xu Q, Zhang QL, Qian H, et al., 2018. Crisis-induced coexisting multiple attractors in a second-order nonautono-

- mous memristive diode bridge-based circuit. *Int J Circ Theor Appl*, 46(10):1917-1927.
<https://doi.org/10.1002/cta.2492>
- Xu Y, Jia Y, Ma J, et al., 2018a. Collective responses in electrical activities of neurons under field coupling. *Sci Rep*, 8(1):1349. <https://doi.org/10.1038/s41598-018-19858-1>
- Xu Y, Jia Y, Ge MY, et al., 2018b. Effects of ion channel blocks on electrical activity of stochastic Hodgkin-Huxley neural network under electromagnetic induction. *Neurocomputing*, 283:196-204.
<https://doi.org/10.1016/j.neucom.2017.12.036>
- Xu Y, Jia Y, Wang HW, et al., 2019. Spiking activities in chain neural network driven by channel noise with field coupling. *Nonl Dynam*, 95(4):3237-3247.
<https://doi.org/10.1007/s11071-018-04752-2>
- Yao Z, Ma J, Yao YG, et al., 2019. Synchronization realization between two nonlinear circuits via an induction coil coupling. *Nonl Dynam*, 96(1):205-217.
<https://doi.org/10.1007/s11071-019-04784-2>
- Ye WJ, Mai WD, Hu GW, 2018. Effects of the electromagnetic radiation on cognitive performance: a model study. *Nonl Dynam*, 93(4):2473-2485.
<https://doi.org/10.1007/s11071-018-4337-4>
- Yu DS, Zheng CY, Iu HHC, et al., 2017. A new circuit for emulating memristors using inductive coupling. *IEEE Access*, 5:1284-1295.
<https://doi.org/10.1109/ACCESS.2017.2649573>
- Yu Y, Zhang C, Han XJ, 2017. Routes to bursting in active control system with multiple time delays. *Nonl Dynam*, 88(3):2241-2254.
<https://doi.org/10.1007/s11071-017-3373-9>
- Zhang YZ, Liu Z, Wu HG, et al., 2019a. Dimensionality reduction analysis for detecting initial effects on synchronization of memristor-coupled system. *IEEE Access*, 7:109689-109698.
<https://doi.org/10.1109/ACCESS.2019.2933252>
- Zhang YZ, Liu Z, Wu HG, et al., 2019b. Two-memristor-based chaotic system and its extreme multistability reconstitution via dimensionality reduction analysis. *Chaos Sol Fract*, 127:354-363.
<https://doi.org/10.1016/j.chaos.2019.07.004>